Proceedings World Geothermal Congress 2026
Calgary, Canada, June 8 – 11, 2026

Analyzing Convective Cells Behavior in Geothermal Reservoirs: Insights and Implications for Resource Development

Giordano Montegrossi[1]*, Mirco Lupi[2] and Maurizio Cei[2]
Istituto di Geoscienze e Georisorse, Consiglio Nazionale delle Ricerche, via G. La Pira 4, Florence, Italy [1]*
Enel Green Power S.p.A., Geothermal Center of Excellence, via A. Pisano 120, Pisa, Italy [2]
giordano.montegrossi@igg.cnr.it

Keywords: Geothermal convection; numerical modeling; reservoir engineering; porous media flow; Rayleigh number; Nusselt number; resource development.

ABSTRACT

In permeable geothermal reservoirs, buoyancy from density changes drives upflow and downflow, so heat transport is dominated by convection rather than conduction. Multiple steady convection states with different Nusselt numbers can coexist, yielding nonhomogeneous temperature fields and variable heat-transfer efficiency. Using reservoir-scale simulations that resolve multiphase flow and heterogeneity, we examine how reservoir curvature, impermeable barriers, and regional inflow reorganize convective cells and affect heat distribution. Curvature focuses upflow beneath structural highs, increasing local thermal gradients; barriers compartmentalize the reservoir, shorten the convective length scale, and reduce overall efficiency; regional inflow imposes throughflow that displaces and merges cells without necessarily increasing domain-averaged heat transfer. These dynamics have direct implications for well siting: production should target upflow beneath structural highs or distal to inflow boundaries, while reinjection benefits from alignment with natural downflow or throughflow. Results emphasize integrating geologic structure and boundary forcing in models to optimize sustainable development.

1 INTRODUCTION

Natural convective circulation is a key mechanism governing heat and mass transport in geothermal reservoirs. In its simplest conceptualization, the system is represented as a homogeneous, permeable layer saturated with fluid and heated from below by magmatic intrusions. Heating decreases fluid density, generating buoyant upflow balanced by descending cooler fluid. This circulation increases shallow temperatures in upflow zones and decreases them in areas of downflow relative to the background thermal gradient, leading to vertically homogenized temperature profiles with subdued gradients relative to conduction-dominated conditions. While conceptually useful, this framework fails to capture natural complexity, which requires more rigorous analysis (Nield and Bejan, 2012).

The systematic investigation of geothermal fluid dynamics began with the pioneering work of Horton and Rogers (1945) and Lapwood (1948), who first applied linear stability analysis to convection in porous media. Their studies demonstrated that convection onset can be predicted through the Rayleigh–Darcy number (Ra), defined under the Boussinesq approximation as:

$$Ra = \frac{\rho_0 g \beta \Delta T H k}{\mu \alpha}$$

where ρ_0 is the reference fluid density, g gravitational acceleration, β the thermal expansion coefficient, ΔT the temperature difference across the layer of thickness H, k the intrinsic permeability, μ the dynamic viscosity, and α the thermal diffusivity of the fluid. Physically, the Rayleigh–Darcy number measures the relative strength of buoyancy, through the density variation $\Delta\rho = \rho_0 \beta \Delta T$, against viscous drag and thermal diffusion. Starting from this framework, Horton and Rogers (1945), and later Lapwood (1948), demonstrated that heat transfer remains diffusion-dominated and the system stable when Ra is below a critical value, whereas buoyancy-driven convection develops and the system becomes unstable once Ra exceeds that threshold. For the classical case of a horizontal porous layer confined between impermeable, isothermal boundaries and with unit aspect ratio, their analysis yielded a critical Rayleigh number of $4\pi^2$, which has since served as a fundamental benchmark for subsequent theoretical and numerical studies. Among such benchmarks, the Elder problem (Elder, 1967) proved particularly influential in demonstrating that multiple steady convection states may coexist, each associated with a distinct heat-transfer efficiency measured by the Nusselt number (Nu). Nu is defined as the

ratio between the total vertical heat flux and the conductive heat flux that would occur in the absence of convection:

$$Nu = \frac{\mathrm{qH}}{\lambda \Delta \mathrm{T}}$$

where q is the mean vertical heat flux and λ the effective thermal conductivity of the fluid. Nu thus captures the degree to which convection augments heat transport. The Elder problem further demonstrated that, even under identical boundary conditions, geothermal reservoirs can sustain circulation modes with variable effectiveness in transporting heat to the surface.

Over subsequent decades, this framework was extended to a wide range of geometrical configurations and boundary conditions, as reviewed comprehensively by Nield and Bejan (2012). Post-onset behavior was initially addressed with perturbation analyses, but the exploration of regimes at high Rayleigh numbers quickly shifted toward numerical approaches, including spectral, finite-difference, and finite-element methods (see O'Sullivan, 2010, for a detailed overview). These studies provided valuable theoretical insights, yet most relied on highly simplified assumptions such as homogeneous permeability, isotropic media, and constant fluid properties under the Boussinesq approximation, conditions far removed from the geological complexity of natural geothermal systems. As a result, they effectively defined the theoretical limits of convection in porous media while highlighting the need for more advanced modeling frameworks capable of addressing reservoir-scale heterogeneity.

A major turning point in the study of geothermal convection occurred in the 1970s with the advent of numerical methodologies capable of simulating non-isothermal, multiphase, and multicomponent flows in heterogeneous and anisotropic porous media. In this period, numerical methods for studying general geothermal flows, including boiling water and steam, were developed and subsequently applied to models of numerous geothermal systems over the following four decades. In particular, the highly nonlinear behavior of boiling zones in high-temperature reservoirs required geothermal simulators to adopt implicit time stepping and upstream weighting of mobilities, approaches that have since become standard (O'Sullivan, 2010). These advances led to the first generation of geothermal reservoir simulators, which over the subsequent decades evolved into indispensable tools for geothermal project design and reservoir management. Beyond large-scale assessments, these simulators have enabled detailed analyses of convective processes, providing new insights into their onset, spatial organization, and morphological evolution under variable reservoir conditions. The incorporation of geological heterogeneity, permeability contrasts, and thermal gradients has further enhanced the realism of these models, allowing systematic evaluation of how local reservoir characteristics shape the geometry and dynamics of convection cells. More recently, high-resolution numerical simulations of statistically steady convection in three-dimensional porous media have extended the accessible range of Rayleigh numbers up to $Ra \approx 2 \times 10^4$. Within this regime, Hewitt et al. (2014) reported that the Nusselt number is well described by a linear fit of the form

$$Nu = \alpha_3 Ra + \beta_3$$

with $\alpha_3 = 9.6 \times 10^{-3}$ and $\beta_3 = 4.6$. This relation confirms the classical trend of increasing heat-transfer efficiency with Rayleigh number and further indicates that, in three dimensions, convective heat transport becomes asymptotically about 40 % more efficient than in two-dimensional systems. These results underscore both the importance of dimensionality and the value of systematic scaling analyses in geothermal convection modeling. Yet, the benefits of increased dimensionality can only be realized if the entire convective system is represented or if boundary conditions are defined in a physically consistent manner. Approximating natural upflow by prescribing artificial heat and mass sources, for instance, can generate spurious behaviors such as stagnant zones where backflow should occur, ultimately distorting the temperature field. These distortions not only bias model calibration but can also propagate into unreliable forecasts of reservoir performance. Extending the computational domain deep enough to include the full circulation system, or apply physically constrained far-field boundary conditions, is therefore essential to avoid such artifacts (Johnson et al., 2022).

Further evidence shows that production and reinjection wells can profoundly reshape convective morphology, modifying circulation pathways and redistributing heat and mass within the reservoir. The extraction of fluids tends to enhance or redirect upflow, while reinjection of cooler water may generate localized downflow, altering the geometry and stability of pre-existing convection cells or even promoting the development of new ones. These interactions highlight the inherently dynamic character of geothermal circulation under exploitation. In such contexts, accurate modeling of convective behavior is useful not only to advance fundamental understanding, but also to provide a practical basis for optimizing well placement, anticipating reservoir

responses, and designing strategies for the sustainable utilization of geothermal resources, thereby underscoring the central role of reservoir modeling in linking fundamental fluid dynamics with applied geothermal engineering.

2 GOVERNING EQUATIONS

The analysis of convective behavior in geothermal reservoirs requires a rigorous mathematical framework describing fluid flow, heat transfer, and their coupling in porous media. We therefore recall the fundamental governing equations that underpin modern geothermal simulators, as presented in O'Sullivan (2010). These formulations provide the framework within which numerical models operate and define the context for investigating the onset, evolution, and modification of convective cells under different structural and boundary forcings.

$$\frac{\partial A_m}{\partial t} + \nabla \cdot F_m = q_m \tag{1}$$

$$\frac{\partial A_e}{\partial t} + \nabla \cdot F_e = q_e \tag{2}$$

where A_m and A_e denote the mass and energy accumulation per unit volume, F_m and F_e the corresponding fluxes, and q_m and q_e the source/sink terms associated with production or injection wells.

For single-phase systems, whether liquid water or steam, the terms are defined as:

$$A_m = \Phi \rho_w \tag{3}$$

$$F_m = \frac{k}{\nu_w}(\nabla p - \rho_w g) \tag{4}$$

$$A_e = (1-\Phi)\rho_r c_r T + \Phi \rho_w u_w \tag{5}$$

$$F_e = h_w F_m - \lambda \nabla T \tag{6}$$

where Φ is porosity, ρ_w fluid density, ν_w kinematic viscosity, p pressure, ρ_r rock density, c_r rock specific heat, T temperature, u_w internal energy of the fluid, h_w enthalpy, and λ the effective thermal conductivity of the saturated porous medium.

For a two-phase mixture of boiling water and steam, the subscripts wl and wv denote liquid water and vapor properties, respectively. Equations from (3) to (6) become:

$$A_m = \Phi(\rho_{wl} S_{wl} + \rho_{wv} S_{wv}) \tag{7}$$

$$F_m = F_{m,wl} + F_{m,wv} \tag{8}$$

$$A_e = (1-\Phi)\rho_r c_r T + \Phi(\rho_{wl} u_{wl} S_{wl} + \rho_{wv} u_{wv} S_{wv}) \tag{9}$$

$$F_e = h_{wl} F_{m,wl} + h_{wv} F_{m,wv} - \lambda \nabla T \tag{10}$$

where S_{wl} and S_{wv} are the liquid and vapor saturations, expressed as volume fractions. To represent two-phase flow, relative permeabilities $k_{r,wl}(S_{wl})$ and $k_{r,wv}(S_{wv})$ are introduced, so that the intrinsic permeability k is scaled by the relative term in computing phase fluxes:

$$F_{m,wl} = \frac{k k_{r,wl}}{\nu_{wl}}(\nabla p - \rho_{wl} g) \tag{11}$$

$$F_{m,wv} = \frac{k k_{r,wv}}{\nu_{wv}}(\nabla p - \rho_{wv} g) \tag{12}$$

Steam–water relative permeabilities are fundamental properties in reservoir engineering and geothermal reservoir simulation, yet their behavior in fractures remains poorly constrained. At high water saturation, steam bubbles become immobile, while water is trapped in pores and fractures at low saturation; the exact values of these residual saturations cannot be measured in situ. Experimental data are scarce and inconsistent, reflecting the difficulty of accounting for phase mass transfer, the very low intrinsic permeability of geothermal reservoir rocks, heat losses in laboratory tests, and the limited understanding of gas–liquid flow mechanisms, including possible gas slippage (Klinkenberg effect). Despite significant research efforts (Li and Horne, 1999;

Gudjonsdottir et al., 2015; Picchi and Battiato, 2020), no universally accepted formulation has yet been established. Reservoir modeling therefore typically relies on generic relative permeability functions, with commonly adopted examples including those of Brooks and Corey (1966), Mualem (1976), Grant (1977), and van Genuchten (1980). Model calibration is then achieved by tuning other parameters to reproduce both natural state conditions and, where available, production data.

Simulation codes implement numerical methods and Equations of State (EOS) that incorporate accurate thermodynamic properties of water in all physical states, ensuring consistent solutions of the governing equations and enabling physically grounded predictions of reservoir behavior, including the dynamics of convective cells (Pruess et al., 1999; O'Sullivan, 2010).

3 CONVECTIVE DYNAMICS IN COMPLEX RESERVOIRS: CASE STUDIES

Convective circulation in geothermal systems rarely develops under idealized homogeneous conditions but is instead shaped by external perturbations that introduce complexity into the flow regime. To investigate these effects, a reference base case was first established and then systematically compared with three scenarios representing variations in reservoir top curvature, impermeable barriers, and regional inflow. Numerical simulations with TOUGH3 (Jung et al., 2017), employing PetraSim for pre- and post-processing (RockWare, 2025), were used to evaluate how each condition influences the stability, geometry, and efficiency of convective heat transfer.

3.1 Base case

In the base configuration, the model represents a simplified hydrothermal system designed to reproduce buoyancy-driven convection under conditions relevant to deep geothermal settings. The circulating fluid is modeled as a binary H_2O–CO_2 mixture containing 3.5 wt.% CO_2, a composition representative of high enthalpy geothermal fluids, allowing for a realistic approximation of fluid density and viscosity.

The model domain spans 15 × 15 km in plan view. The structured Cartesian mesh consists of 158,804 elements distributed over 29 vertical layers. Vertical discretization is refined within the reservoir to resolve boundary layers and gradients while preserving computational efficiency.

The main material properties adopted for the model are summarized in Table 1.

Table 1. Main material properties adopted in all model scenarios

Property	Heat source	Reservoir	Cap rock
Porosity	0.03	0.03	0.05
Permeability [m^2]	$1{\cdot}10^{-16} \div 1{\cdot}10^{-33}$	XY: $1{\cdot}10^{-15}$ Z: $5{\cdot}10^{-15}$	$1{\cdot}10^{-33}$
Specific heat capacity $\left[\frac{J}{kg{\cdot}K}\right]$	∞	2500	2500
Thermal conductivity $\left[\frac{W}{m{\cdot}K}\right]$	2	3	3
Density $\left[\frac{kg}{m^3}\right]$	2600	2700	2650

Within the vertical column, the reservoir portion, corresponding to the most permeable and thermally active interval, has a uniform thickness of 1900 m. Permeability in this layer is assigned sufficiently high values to promote the onset of convective motion, whereas the overlying and underlying formations are characterized by low permeability and act as thermal and hydraulic barriers confining circulation within the reservoir zone. An infinite heat capacity is assigned to the basal heat source, allowing it to maintain a constant temperature irrespective of upward heat transfer. This assumption effectively decouples the thermal evolution of the source from that of the overlying domain, ensuring a persistent thermal driving force for convection.

All lateral boundaries are closed to both mass and heat flux, so that circulation is driven solely by buoyancy. Relative permeabilities are calculated using the van Genuchten correlations, providing a smooth transition between liquid- and vapor-dominated flow regimes while maintaining numerical stability in two-phase conditions.

The system is initialized under purely conductive thermal conditions defined by fixed temperatures at the top and bottom boundaries and evolved in time until a statistically steady convective configuration is reached. Under these conditions, the system's Rayleigh number corresponds to the steady three-dimensional roll regime described by Hewitt et al. (2014), in which convective circulation organizes into stable, laterally periodic cells (Figure 1).

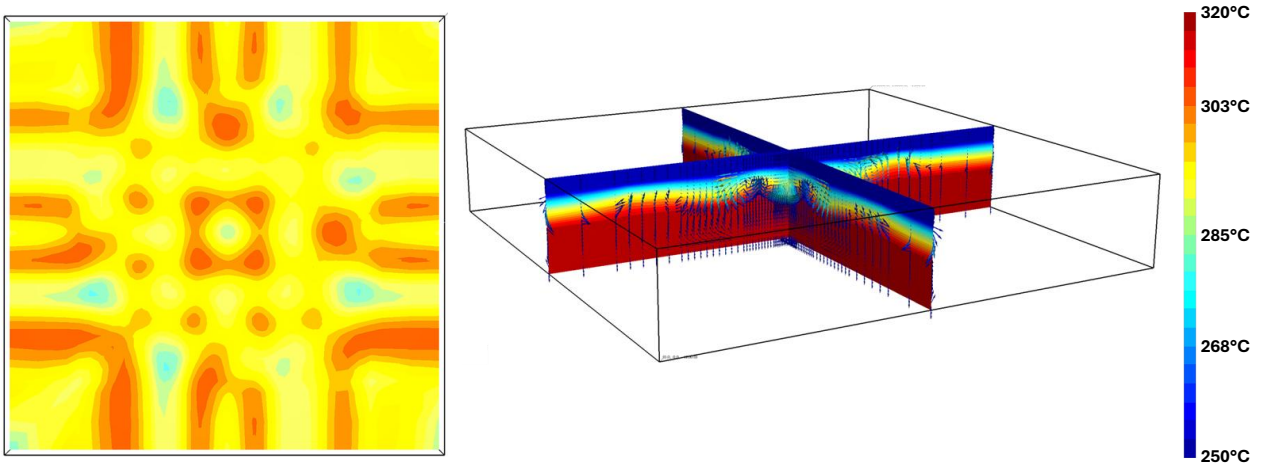


Figure 1. Temperature distribution for the flat-domain configuration (top boundary 250 °C, bottom boundary 320 °C). Left: plan-view map at −2500 m depth. Right: cross-sectional view along the X and Y axes (sections at 7500 m) with flow vectors.

In plan view, the steady-state temperature distribution exhibits a multicellular convective pattern with alternating hot and cold regions corresponding to upflow and downflow zones, respectively. The cells display a quasi-symmetric organization around the domain center, forming polygonal roll structures typical of stable 3D convection. Toward the domain margins, the rolls become slightly elongated and aligned parallel to the boundaries, indicating a mild geometric constraint imposed by the closed boundary conditions. The overall configuration confirms that thermal energy is efficiently redistributed through buoyancy-driven circulation, maintaining a dynamic but steady convective equilibrium.

The model described provides the reference state from which the sensitivity of convective structures to geological and boundary perturbations can be systematically explored.

3.2 Effect of reservoir-top curvature

Curved reservoir tops are common in many geothermal systems worldwide, reflecting the combined influence of tectonic deformation and shallow magmatic intrusion. Well-documented examples include Wairakei (New Zealand), Olkaria and Menengai (Kenya), all hosted in extensional volcanic settings (Rosenberg et al., 2009; Omenda, 1998; Montegrossi et al., 2015), as well as Larderello and Monte Amiata (Italy) and the Japanese systems of Unzen and Aso, developed in convergent or subduction-related domains (Gianelli et al., 1988; Bertini et al., 2006; Kagiyama et al., 1999; Kanda et al., 2019). To evaluate the influence of such geometry on convective behavior, the reservoir top was modeled with a convex curvature whose apex lies 600 m above the flat reference configuration. All other physical and thermodynamic parameters were kept constant, allowing the assessment of how structural curvature modifies the organization of convective circulation. The resulting temperature distribution is shown in Figure 2.

Compared to the flat reference model (Figure 1), the curved-top model (Figure 2) shows a marked concentration of the thermal field beneath the structural apex. The curvature enhances vertical heat transfer, producing a broad central upflow zone and suppressing the lateral alternation of hot and cold regions observed in the flat case. The 600 m uplift increases the effective layer thickness, yielding a slightly higher Rayleigh–Darcy number and a more focused, asymmetric convective structure. As a result, the thermal energy flux reaching the top of the reservoir becomes more localized and intense beneath the apex, while it decreases along the flanks where downflow dominates. This focusing redistributes the upward energy flow, concentrating it in large central upflow zone and enhancing local thermal gradients near the curved cap. This is consistent with convection-dominated geothermal systems as described by Moeck (2014), in which the structural and permeability architecture controls the spatial distribution of upflow and discharge zones. When the reservoir domain is structurally curved due to tectonic or intrusive processes and sufficient permeability is available, the principal upflow is expected

to develop near the structural high, emphasizing the fundamental role of structural relief in focusing convective discharge and sustaining geothermal circulation.

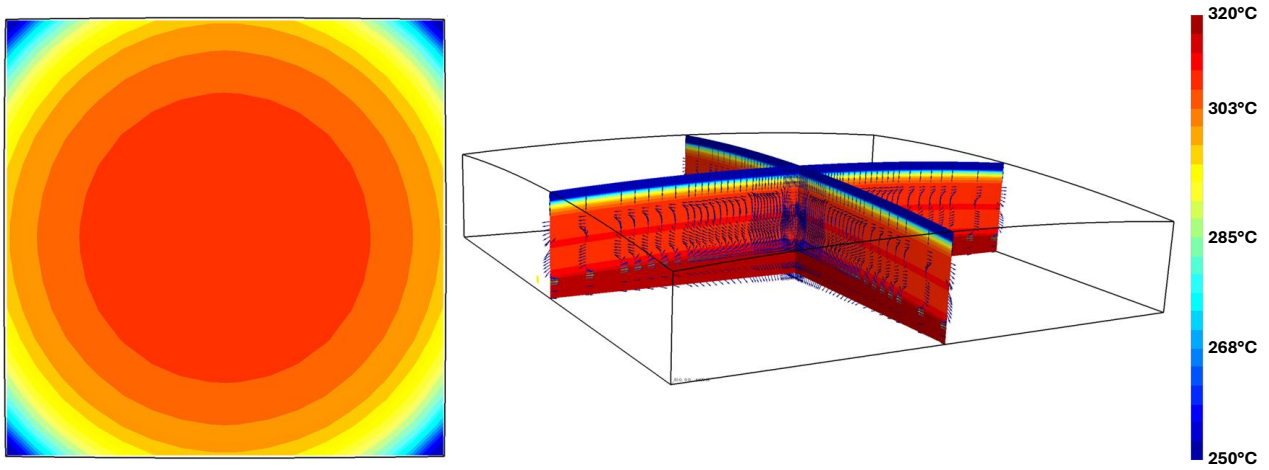


Figure 2. Temperature distribution for the curved-top scenario. Left: plan-view map at −2000 m depth. Right: cross-sectional view along the X and Y axes (sections at 7500 m) with flow vectors.

Compared to the flat reference model (Figure 1), the curved-top model (Figure 2) shows a marked concentration of the thermal field beneath the structural apex. The curvature enhances vertical heat transfer, producing a broad central upflow zone and suppressing the lateral alternation of hot and cold regions observed in the flat case. The 600 m uplift increases the effective layer thickness, yielding a slightly higher Rayleigh–Darcy number and a more focused, asymmetric convective structure. As a result, the thermal energy flux reaching the top of the reservoir becomes more localized and intense beneath the apex, while it decreases along the flanks where downflow dominates. This focusing redistributes the upward energy flow, concentrating it in large central upflow zone and enhancing local thermal gradients near the curved cap. This is consistent with convection-dominated geothermal systems as described by Moeck (2014), in which the structural and permeability architecture controls the spatial distribution of upflow and discharge zones. When the reservoir domain is structurally curved due to tectonic or intrusive processes and sufficient permeability is available, the principal upflow is expected to develop near the structural high, emphasizing the fundamental role of structural relief in focusing convective discharge and sustaining geothermal circulation.

From a resource development perspective, this configuration is favorable for geothermal exploitation: if the structural high is correctly identified, wells drilled near the apex can intersect the high enthalpy upflow zone at shallower depths, accessing hotter fluids with reduced drilling costs. At the same time, reinjection at the flanks of the structural high is advantageous, as the injected fluid naturally follows the descending limbs of the convective circulation, thereby supporting the natural sweeping of the downflow zones. Structural curvature thus enhances both the thermodynamic efficiency of convection and the economic viability of resource utilization.

3.3 Impermeable barriers

Impermeable or low-permeability barriers are common features in geothermal reservoirs and can exert strong control on the geometry and efficiency of convective circulation. They may originate from lithological contrasts, self-sealing due to mineral deposition, or the presence of fault zones with reduced transmissivity. Such discontinuities compartmentalize the flow domain, modify pressure gradients, and often distort the symmetry of otherwise regular convective cells (Grant and Bixley, 2011). Comparable compartmentalization has been documented in several active geothermal systems worldwide, including Los Humeros (Mexico), where resistivity and seismic data reveal sealing faults that subdivide the reservoir into distinct blocks (Flores et al., 2022; Kennedy et al., 2022; Weydt, 2023); Krafla (Iceland), where hyaloclastite units and caldera-bounding structures act as lateral flow barriers (Árnáson, 2020; Scott et al., 2019); and Kamojang (Indonesia), where tracer and microseismic monitoring indicate limited inter-well connectivity consistent with partial hydraulic isolation (Budiardjo et al., 2002; Abidin et al., 2009; Hendriansyah and Wicaksono, 2015). To assess their influence, the base model was modified by introducing four impermeable barriers within the reservoir layer. Two barriers are oriented vertically and two horizontally, each spaced at 5 km intervals and extending across the entire 15 × 15 km domain. Together, they subdivide the convective zone into nine hydraulic sectors. Each barrier is continuous throughout the reservoir thickness but contains a small central aperture that allows limited hydraulic

communication between adjacent compartments. These barriers locally inhibit fluid exchange but maintain weak interconnection between cells. All other physical and boundary conditions were kept identical to the base case to isolate the effect of flow obstruction. The resulting temperature distribution at −2500 m depth is shown in Figure 3.

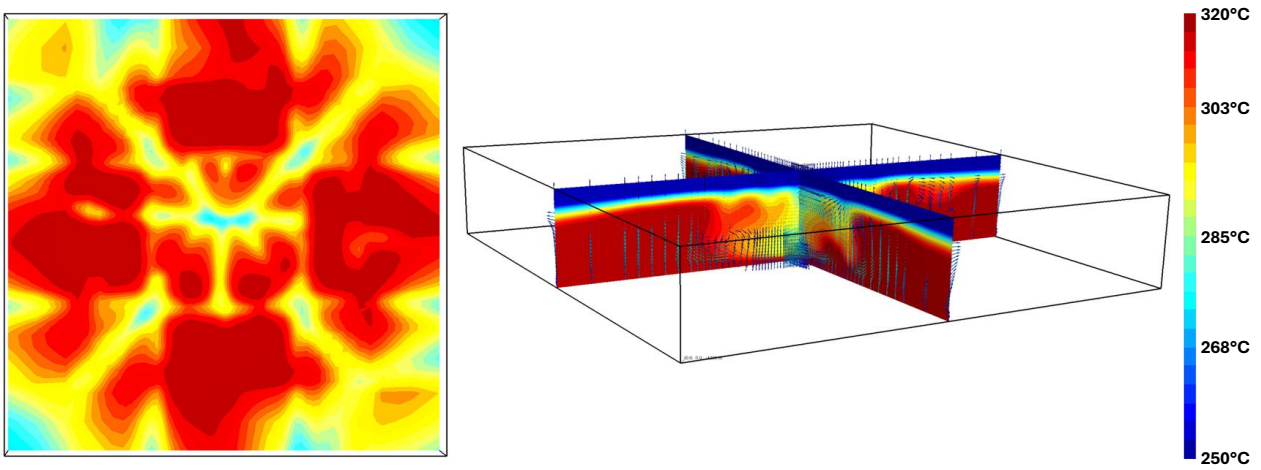


Figure 3. Temperature distribution for the impermeable barriers scenario. Left: plan-view map at −2500 m depth. Right: cross-sectional view along the X and Y axes (sections at 7500 m) with flow vectors.

Compared to the unperturbed configuration (Figure 1), the introduction of impermeable barriers produces a fragmented convective pattern, with smaller and thermally less efficient cells. The high-temperature zones become laterally discontinuous, and cooler regions develop immediately downstream of the barriers, where circulation is suppressed. The presence of the barriers effectively reduces the horizontal characteristic length of the system, leading to a lower Rayleigh–Darcy number and a weaker convective regime. Although limited hydraulic communication occurs through the central apertures, the barriers prevent the full development of lateral convection cells, allowing only orthogonal mass fluxes between compartments. In the corner sectors, convection is largely absent due to the small characteristic length and the dominance of downflow diverted from the central zones. As a result, the overall heat-transfer efficiency declines relative to the base case, as indicated by a reduced Nusselt number and smoother lateral temperature gradients. This behavior is partly consistent yet conceptually divergent from the framework proposed by Moeck (2014). While Moeck emphasizes the role of structural and permeability architecture in focusing and sustaining convective upflow in geothermal plays, the present results show that when such structures evolve into impermeable barriers, they instead disrupt lateral connectivity and suppress large-scale convection. In this configuration, the reservoir departs from the efficient circulation regimes typical of fully developed, convection-dominated systems, shifting toward a compartmentalized and less thermally effective configuration.

From a resource development perspective, the presence of internal barriers implies a more complex hydraulic architecture that can strongly influence well performance and inter-well communication. In a conventional geothermal development strategy, production wells should be ideally located above the main upflow zone, where the highest-enthalpy fluids are expected, while reinjection wells are generally placed in cooler downflow areas to sustain circulation. In practice, however, the exact position of the upflow is rarely well constrained, and structural compartmentalization further complicates its identification. When impermeable barriers separate the upflow from the downflow sectors, the natural connection between production and reinjection zones can be disrupted. As a result, reinjected fluids may not effectively recharge the productive volume, leading to poor pressure support and longer fluid return times. In such conditions, defining the optimal well layout becomes particularly challenging, and reinjection within or near the upflow region may sometimes represent the most reliable strategy to ensure that injected fluids contribute to sustaining production.

3.4 Regional inflow

Regional groundwater inflows are common in many geothermal systems, where large-scale hydraulic gradients or deep recharge from adjacent formations interact with local convective circulation. Such lateral inputs can enhance, distort, or even suppress existing convective cells depending on their magnitude, direction, and temperature relative to the resident fluid (Grant and Bixley, 2011; Moeck, 2014). Similar patterns have been observed in natural geothermal systems such as Rotokawa (New Zealand) and Hveragerði (Iceland), where regional inflow interacts with buoyancy-driven circulation and shapes asymmetric upflow zones (Wallis et al.,

2013; Clearwater et al., 2010; Suryanto, 2021; Mutonga et al., 2010). To investigate these effects, a lateral cold inflow of 68 kg/s was imposed as a mass flux boundary condition along the upper-right edge of the model domain, extending over 15 km of the reservoir boundary. The inflow represents external recharge from the regional aquifer. All other parameters were kept constant to isolate the effect of lateral flow. The resulting temperature field at −2500 m depth and the corresponding vertical slice across the inflow path are shown in Figure 4.

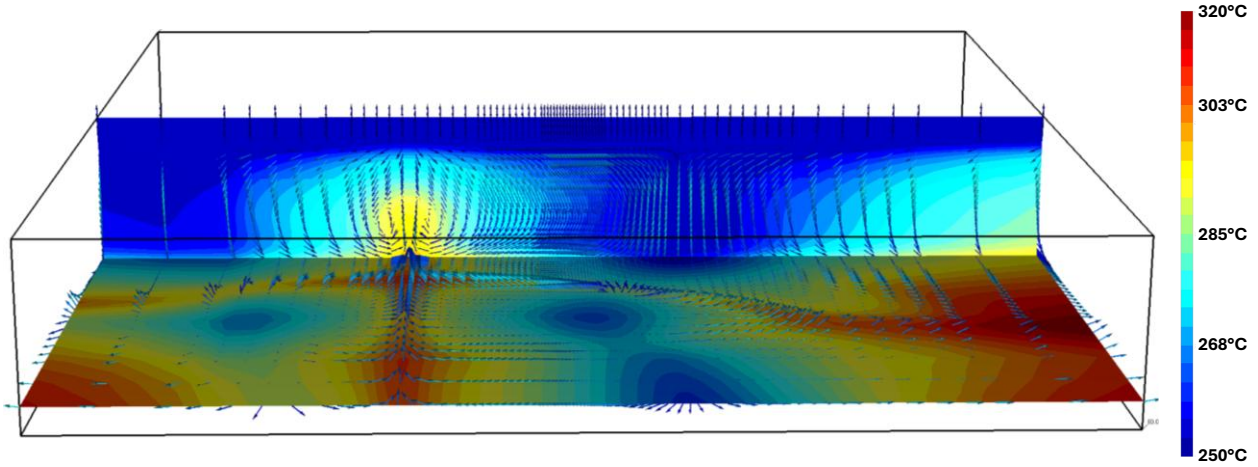


Figure 4. Temperature distribution at −3500 m depth and vertical cross section at 7500 m on X with flow vectors, for the regional inflow scenario.

The lateral recharge drives a unidirectional throughflow that interacts with the buoyancy-driven convection, breaking the spatial symmetry observed in the base case (Figure 1). The inflowing fluid introduces a strong temperature gradient across the domain, with cooler conditions near the inflow boundary and progressive heating toward the opposite side. As a result, the convective cells are displaced downflow, merging into an asymmetric composite circulation characterized by a broad upflow zone on the distal side and a weakened counterflow upstream. From a quantitative standpoint, this configuration corresponds to a mixed forced–buoyancy regime, where the imposed lateral inflow introduces an advective component to the circulation while the Rayleigh number remains unchanged. As a result, convective structures are redistributed rather than intensified, and the domain-averaged Nusselt number remains comparable to the base case, despite localized enhancement near the distal upflow and attenuation along the inflow margin.

From a development perspective, the presence of regional inflow fundamentally alters the logic of well placement. In the previous scenarios, optimal production and reinjection strategies could be defined with respect to the location of upflow and downflow zones within the convective pattern. Here, however, the imposed regional recharge disrupts cell symmetry and establishes a dominant throughflow that overrides local convection. As a consequence, drilling targets can no longer be selected solely based on thermal anomalies but must instead be aligned with the direction and extent of the inflowing fluid. If the inflow is sufficiently warm and compatible in composition, it can sustain reservoir pressure and extend the productive lifespan of the system; conversely, if it introduces colder or chemically distinct fluids, it may induce cooling and compositional changes within the upflow. Therefore, accurately constraining the magnitude, temperature, and geometry of regional recharge becomes essential for identifying the most productive areas and for designing reinjection strategies that operate in concert with, rather than against, the natural hydraulic regime.

4 CONCLUSIONS

The numerical analyses presented here demonstrate that structural geometry, permeability distribution, and boundary conditions exert first-order control on the organization and efficiency of convective circulation in geothermal reservoirs. Even subtle geometric or hydraulic perturbations can markedly alter the location, intensity, and stability of upflow and downflow zones, thereby influencing both thermal performance and optimal development strategy.

In the base configuration, buoyancy-driven convection organizes into stable polygonal rolls typical of high-Rayleigh 3D systems. In such reservoirs, production and reinjection wells should ideally be positioned above the upflow and downflow zones, respectively, so that artificial circulation reinforces the natural convective pattern, representing the reference state of an efficient geothermal system. When reservoir-top curvature is introduced,

heat transfer becomes focused beneath the structural high. The enhanced vertical gradients and localized upflow make the apex the most favorable target for production drilling, while reinjection along the flanks supports the descending limbs of convection. Structural curvature thus enhances both thermodynamic efficiency and economic viability. The introduction of impermeable barriers fragments the reservoir into compartments, reducing the characteristic length of circulation and overall heat-transfer efficiency. The resulting poor hydraulic connectivity may prevent reinjected fluids from recharging the productive upflow. Under such conditions, reinjection closer to or even within the upflow zone may better sustain pressure and thermal output. When regional inflow dominates, convection is replaced by a throughflow regime in which the external hydraulic gradient governs the main flow path. Field development must therefore align wells with the direction and magnitude of recharge rather than the convective pattern: drilling near the inflow enhances recharge, while reinjection along the throughflow minimizes thermal interference.

Overall, these results show that the interaction between structure and boundary forcing defines not only the morphology of geothermal convection but also the operational framework for sustainable resource utilization. Integrating geological and hydrodynamic modeling is essential to identify productive drilling zones, optimize reinjection, and ensure long-term reservoir performance.

REFERENCES

Lapwood, E.R.: Convection of a fluid in a porous medium, *Mathematical Proceedings of the Cambridge Philosophical Society,* 44, (1948), 508-521.

Horton, C.W., and Rogers, F.T.: Convection currents in a porous medium, *Journal of Applied Physics*, 16.6, (1945), 367-370.

Johnson, P.J., Stauffer, P.H., Omagbon, J., and Moore, C.R.: Implications of rootless geothermal models: missing processes, parameter compensation, and imposter convection, *Geothermics*, 102, (2022), 102391.

Picchi, D., and Battiato, I.: Scaling of two-phase water-steam relative permeability and thermal fluxes in porous media, *International Journal of Multiphase Flow*, 129, (2020), 103257.

Elder, J.W.: Transient convection in a porous medium, *Journal of Fluid Mechanics*, 27.3, (1967), 609–623.

Gudjonsdottir, M., Palsson, H., Eliasson, J., and Saevarsdottir, G.: Calculation of relative permeabilities from field data and comparison to laboratory measurements, *Geothermics*, 54, (2015), 1–9.

Hewitt, D.R., Neufeld, J.A., and Lister, J.R.: High Rayleigh number convection in a three-dimensional porous medium, *Journal of Fluid Mechanics*, 748, (2014), 879–895.

Li, K., and Horne, R.N.: Accurate measurement of steam flow properties, *Proceedings of 1999 GRC Annual Meeting*, Reno, Nevada (1999).

Nield, D.A., and Bejan, A.: Convection in porous media, 4th edition, Springer New York, (2012).

O'Sullivan, M.J.: Geothermal fluid dynamics, *Proceedings of 17th Australasian Fluid Mechanics Conference*, Auckland, New Zealand (2010).

Pruess, K., Oldenburg, C.M., and Moridis, G.J.: TOUGH2 user's guide version 2.0, (1999).

Jung, Y., Pau, G.S.H., Finsterle, S., and Pollyea, R.M.: TOUGH3: a new efficient version of the TOUGH suite of multiphase flow and transport simulators, *Computers & Geosciences*, 108, (2017), 2-7.

RockWare: PetraSim user manual, (2025). Available at: https://www.rockware.com/petrasim-documentation (Accessed: 2025-10-03)

van Genuchten, M.T.: A closed form equation for predicting the hydraulic conductivity of unsaturated soils, *Soil Science Society of America Journal*, 44.5, (1980), 892-898.

Brooks, R.H., and Corey, A.T.: Properties of porous media affecting fluid flow, *Journal of the Irrigation and Drainage Division*, 92.2, (1966), 61-88.

Mualem, Y.: A new model for predicting the hydraulic conductivity of unsaturated porous media, *Water Resources Research*, 12.3, (1976), 513-522.

Grant M.A.: Permeability reduction factors at Wairakei, *Proceedings of the AIChE-ASME Heat Transfer Conference*, Salt Lake City, Utah (1977).

Rosenberg, M.D., Bignall, G., and Rae, A.J.: The geological framework of the Wairakei–Tauhara geothermal system, New Zealand, *Geothermics*, 38.1, (2009), 72–84.

Omenda, P.A.: The geology and structural controls of the Olkaria geothermal system, Kenya, *Geothermics*, 27.1, (1998), 55–74.

Montegrossi, G., Pasqua, C., Battistelli, A., Mwawongo, G., and Ofwona, C.: 3D natural state model of the Menengai geothermal system, Kenya, *Proceedings of the World Geothermal Congress*, Melbourne, Australia (2015).

Bertini, G., Casini, M., Gianelli, G., and Pandeli, E.: Geological structure of a long-living geothermal system, Larderello, Italy, *Terra Nova*, 18.3, (2006), 163–169.

Gianelli, G., Puxeddu, M., Batini, F., Bertini, G., Dini, I., Pandeli, E., and Nicolich, R.: Geological model of a young volcano-plutonic system: the geothermal region of Monte Amiata (Tuscany, Italy), *Geothermics*, 17.5-6, (1988), 719–734.

Kagiyama, T., Utada, H., and Yamamoto, T.: Magma ascent beneath Unzen Volcano, SW Japan, deduced from the electrical resistivity structure, *Journal of Volcanology and Geothermal Research*, 89.1–4, (1999), 35–42.

Kanda, W., Utsugi, M., Takakura, S., and Inoue, H.: Hydrothermal system of the active crater of Aso volcano (Japan) inferred from a three-dimensional resistivity structure model, *Earth, Planets and Space*, 71.1, (2019), 37.

Moeck, I.S.: Catalog of geothermal play types based on geologic controls, *Renewable and Sustainable Energy Reviews*, 37, (2014), 867-882.

Grant, M.A., and Bixley, P.F.: Geothermal reservoir engineering, 2nd edition, Academic Press, (2011).

Flores, C., Aviles Esquivel, T., Arango-Galván, C., and Salas J.L.: Seal cap resistivity structure of Los Humeros geothermal field from direct current and transient electromagnetic soundings, *Geofísica Internacional*, 61.4, (2022), 351-376.

Kennedy, H., Löer, K., and Gilligan, A.: Constraints on fracture distribution in the Los Humeros geothermal field from beamforming of ambient seismic noise, *Solid Earth*, 13.12, (2022),1843–1858.

Weydt, L.M.: The Los Humeros volcanic complex – structure, evolution and geothermal potential, PhD thesis, (2023), TU Darmstadt.

Árnáson, K.: New conceptual model for the magma-hydrothermal system of Krafla, NE Iceland. *Geosciences*, 10.1, (2020), 34.

Scott, S.W., Covell, C., Júlíusson, E., Valfells, Á., Newson, J., Hrafnkelsson, B., Pálsson, H., and Gudjónsdóttir, M.: A probabilistic geologic model of the Krafla geothermal system, *Geothermal Energy*, 7, (2019), 26.

Budiardjo, M., Thamrin, H., and Abidin, N.Z.: Reinjection wellsetting study at the Kamojang geothermal field based on geochemical tracer and micro-seismic data, *Proceedings of the 31st Annual Convention of Indonesian Association of Geologists*, Surabaya, Indonesia (2002).

Abidin, N.Z., Prasetio, R., and Prayoto, P.: Geothermal reservoir characterization for steam field management in Kamojang geothermal field, West Java, *Atom Indonesia*, 35.1, (2009), 37-48.

Hendriansyah, T., and Wicaksono, T.: Tracing reinjected condensate using microearthquake monitoring at the Kamojang geothermal field, *Proceedings of the World Geothermal Congress*, Melbourne, Australia (2015).

Wallis, I.C., Bardsley, C., Powell, T., Rowland, J.V., and O'Brien J.M.: A structural model for the Rotokawa geothermal field, New Zealand, *Proceedings of the 35th New Zealand Geothermal Workshop*, Auckland, New Zealand (2013).

Clearwater, E.K., O'Sullivan M.J.: Large-scale natural convection in the Wairakei–Tauhara geothermal field, *Proceedings of the 17th Australasian Fluid mechanics conference*, Auckland, New Zealand (2010).

Suryanto, R.: Geological modelling of the Hveragerði Geothermal System, SW Iceland. United Nations University Geothermal Training Programme, Iceland, 26, (2021).

Mutonga, M.W., Sveinbjornsdottir, A., Gislason, G., and Ármannsson, H.: The isotopic and chemical characteristics of geothermal fluids in the Hengill Area (Hellisheiði, Hveragerði, and Nesjavellir fields), SW-Iceland, *Proceedings of the World Geothermal Congress*, Bali, Indonesia (2010).